FULL PAPER

Chlorine-Sensing Chips

ADVANCED
MATERIALS
INTERFACES

www.advmatinterfaces.de

A Novel Sensing Chip for Probing Chlorine Permeation into Simulated Produce Cracks

Yongguang Guan, Yaguang Luo, Zi Teng, Bin Zhou, Lei Mei, Gary R. Bauchan, and Qin Wang*

Pathogen inactivation efficacy is substantially lower on cracks/crevices than on smooth produce surfaces. In this study, an interlocking design of three-dimensionally printed chip coated with zein-*N*,*N*-diethyl-p-phenylenediamine (DPD) film is developed to study chlorine permeation in simulated cracks. The primary interaction of zein and DPD in film is hydrogen bonding evidenced by the blue shift of the amide II band of zein. The chlorine-sensing chip exhibits a dose-dependent magenta color change upon immersion in chlorine solutions. Lab-scale experiment is performed on chips with full-depth cracks. At crack widths of 0.2, 0.5, and 1.0 mm, respectively. The static chlorine permeation distances are 11.6, 15.3, and 20.0 mm, when the cracks are perpendicular to the liquid level, compared to 0, 3.3, and 4.3 mm when the cracks are parallel to the liquid level. Complete permeation was detected after dynamic washing for 30 s at chlorine solution *Re* numbers of 12.5 and 125. In a pilot-industrial scale washer, chlorine-permeated distance of 20 mm is detected for full-depth chlorine-sensing chips, and 0, 9.4, and 20 mm for half-depth chips at width of 0.2, 0.5, and 1.0 mm, respectively. Results demonstrated that gravity and boundary pressure facilitates chlorine permeation. This work provides a potential platform for studying the accessibility of sanitizers in narrow gaps under lab-/industry-relevant conditions.

1. Introduction

Consumption of fresh produce contaminated with human pathogens has become a leading cause of food-borne illness.[1]

Dr. Y. Guan, Dr. Z. Teng, L. Mei, Dr. Q. Wang
Department of Nutrition and Food Science
University of Maryland
College Park, MD 20742, USA
E-mail: wangqin@umd.edu
Dr. Y. Guan, Dr. Y. Luo, Dr. Z. Teng, Dr. B. Zhou
Environmental Microbial and Food Safety Laboratory
United States Department of Agriculture
Agricultural Research Service
Beltsville, MD 20705, USA
Dr. Y. Guan, Dr. Y. Luo, Dr. Z. Teng, Dr. B. Zhou
Food Quality Laboratory
United States Department of Agriculture
Agricultural Research Service
Beltsville, MD 20705, USA
Dr. G. R. Bauchan
Electron and Confocal Microscope Unit
United States Department of Agriculture
Agricultural Research Service
Beltsville, MD 20705, USA

Cracks and crevices on fresh produce are sites where pathogens can adhere, colonize, and attach and are protected to some degree from sanitizers.[2] These irregularities on the produce surfaces reduce the efficacy of pathogen inactivation by antimicrobial agents. The importance of these physical features in relation to food safety is well recognized. However, the lack of a suitable technology to detect the permeation of antimicrobial agents into cracks and crevices is a restriction to develop intervention technologies for pathogen inactivation, which could compromise the food safety and public health. A novel 3D printed chlorine-sensing chip with simulated cracks was thus developed to address these critical food safety knowledge gaps.

The 3D printing technology has advanced significantly in the last two decades. Applications range from material science,[3] biomedical field,[4] especially for bionic models,[5] intellectualized chip development,[6] (bio)analytical,[7] and biosensor[8] technologies. Generally, various thermoplastic materials such as polylactic acid (PLA), acrylonitrile butadiene styrene (ABS), polycarbonate (PC), and polyamide (PA) have been used for 3D printing.[9] Among these materials, PLA has been frequently applied owing to its thermoplastic and biodegradable nature, high biological and solvent compatibility, and favorable plasticity.[10] Additionally, the 3D models have been broadly employed in mimicking the natural produce surface,[11] with various surface morphologies and physicochemical properties such as bone scaffold,[12] and cell carrier.[13]

Chlorine is an antimicrobial agent that has been most widely used in the fresh produce industry.[14] The *N*,*N*-diethyl-p-phenylenediamine (DPD) is commonly used to determine free chlorine concentration via a colorimetric approach due to its reaction with chlorine to form a magenta-colored intermediate product, a semiquinoid cationic compound.[15] Zein, a major protein from maize, comprises four major polymer components with known molecular weight of 9.6, 13.5, 21.0, and 23.0 kDa, respectively.[16] Its abundance of hydrophobic amino acids such as leucine and proline makes zein a good film former,[16] while the high content of tyrosine residues (≈5.0% w/w) provides potential binding sites to DPD through various mechanisms including hydrophobic interaction,[17] hydrogen bonds,[18] and possible π–π interaction [π-stacking] and p–π interaction.[19]

ADVANCED
SCIENCE NEWS
www.advancedsciencenews.com

ADVANCED
MATERIALS
INTERFACES
www.advmatinterfaces.de

These features make zein a promising stabilizer to generate a film with embedded DPD.

The main objectives of this study are to 1) develop and fabricate a chlorine-sensing chip using 3D printed materials for assembling models that simulate produce cracks and crevices found in fresh produce; 2) characterize the physicochemical properties of this chlorine-sensing chip, including surface properties and molecular interaction mechanism; and 3) investigate the dynamic response of the fabricated chip in the presence of chlorine, and chlorine permeation into model cracks in both lab- and pilot-industrial scale produce washing systems.

2. Results and Discussion

2.1. Interface Properties of Chlorine-sensing Chip

A PLA-based chip was first fabricated by 3D printing as a model for mimic cracks present on produce. Then, a layer of DPD@zein film was coated onto the "male" surface of the base chip to sense chlorine. Both the 3D printed PLA base chip and the chip coated with DPD@zein layer exhibited a waved, but relatively smooth topography, with average roughness of 52.3 (base) and 79.3 μm (coated), respectively (**Figure 1**a,b).

Surface and internal topographical features of the DPD@zein layer were observed using a FIB/SEM and shown in **Figure 2**a. The microstructure of the DPD@zein film consisted of spherical particles across the film, which was typical for a dried zein coating. Moreover, the average thickness of the DPD@zein layer was 60 μm which, together with the smoothness, made the film suitable for studying the permeation of chlorine solution without physical steric hindrance.

Wettability of the base chip and chlorine-sensing chip surfaces was presented in Figure 2b,c. The contact angles of water droplets on uncoated and coated chips were measured at 96.1° and 43.8°, respectively, suggesting decreased hydrophobicity and greater wettability of the coated chip by aqueous solutions. Similarly, a contact angle of 39.7° was observed for a chlorine solution (72 mg L^{-1} FAC) on the coated chip surface. A more hydrophilic layer on the surface of chlorine-sensing chip allowed free chlorine to contact and react readily with the DPD reagent embedded in the zein film. On the other hand, the contact angle of DPD–zein-70% ethanol solution on the base chip surface was 21.4°. This demonstrated that the PLA base was capable of being equably coated with the DPD–zein-70% ethanol solution. The affinity of the coating solution to PLA could be ascribed to the Cassie-Wenzel wetting transition occurring on the interface of the PLA surface,[20] which suggested significant attraction between the base and the DPD@zein film, resulting in uniform diffusion of coating solution on base chip surface to form same thickness of layer.

2.2. Intermolecular Interaction between DPD and Zein

Fluorescence spectrophotometry is a convenient tool to study the interactions between biomolecules. Fluorescence is typically observed when the fluorophore of a molecule is partially or fully blocked.[21,22] Fluorescence spectra of DPD–zein solution

revealed a maximum absorption peak at 305 nm (**Figure 3**a–c), most likely due to the presence of tyrosine, the primary fluorescent chromophoric group in zein.[23] After the addition of DPD, the fluorescence intensity of zein was significantly decreased, suggesting an interaction between chromophoric groups and DPD molecules. This may involve both dynamic and static mechanisms, i.e., intermolecular collision and generation of stable complexes.

The fluorescence quenching data were further analyzed using the Stern–Volmer model (Equation (1)).[24]

$$\frac{F_o}{F} = 1 + k_q \tau_o [Q] \tag{1}$$

where F_o and F are the fluorescence intensities without and with a quencher, respectively, $[Q]$ is the concentration of the quencher (M), k_q is the biomolecular quenching constant, and constant τ_o (= 3 ns) is the average life span of fluorophore without a quencher.

As calculated from the data in Figure 3d, the quenching constant (k_q value) of DPD to zein was 6.8×10^{10} M^{-1} s^{-1} at 25 °C. Elevating the temperature resulted in an increase of the k_q value to 8.2×10^{10} and 10.1×10^{10} M^{-1} s^{-1} at 35 and 45 °C, respectively (Figure 3d), suggesting a steady increase in the content of DPD–zein complexes.[23] Based on the quenching mechanism with the measured k_q value higher than 2.0×10^{10} M^{-1} s^{-1}, the predominant cause of fluorescence quenching of zein by DPD was the formation of stable DPD–zein complexes.[22]

For the static quenching (forming complexes), the binding constant K_a and binding sites n of DPD to the fluorophore of zein were calculated according to the following Equation (2)[25]

$$\log \left[\frac{F_o - F}{F} \right] = \log K_a + n \log [Q] \tag{2}$$

where the value of binding constant K_a can be obtained from the intercept with the y-axis of the plot of $\log \left[\frac{F_o - F}{F} \right]$ against $\log[Q]$, and the value of binding sites n can be obtained from the slope (Figure 3e).

Both the binding constant K_a and binding sites n are shown in **Table 1** as a function of temperature. The increased binding constant for DPD and zein indicated enhanced complex stability and greater hydrophobic interaction at higher temperatures.[23] Additionally, the n values were close to 1 at all temperatures, which suggested an approximate equimolar binding between DPD and zein molecules under the tested conditions.

The K_a values of DPD–zein complexes were further employed to derive the change in enthalpy (ΔH), entropy (ΔS), and Gibbs free energy (ΔG) to reveal the thermodynamic interactions. Possible interactions including electrostatic attraction, hydrogen bonds, van der Waals interaction, and hydrophobic interaction,[26] can typically be modeled by the Van't Hoff plot (Equations (3) and (4))

$$\ln K_a = -\frac{\Delta H}{RT} + \frac{\Delta S}{R} \tag{3}$$

$$\Delta G = \Delta H - T\Delta S \tag{4}$$

where R is the gas constant of 8.314 J (mol K)$^{-1}$, and T (K) is the experimental temperature. The theoretical values ΔH and
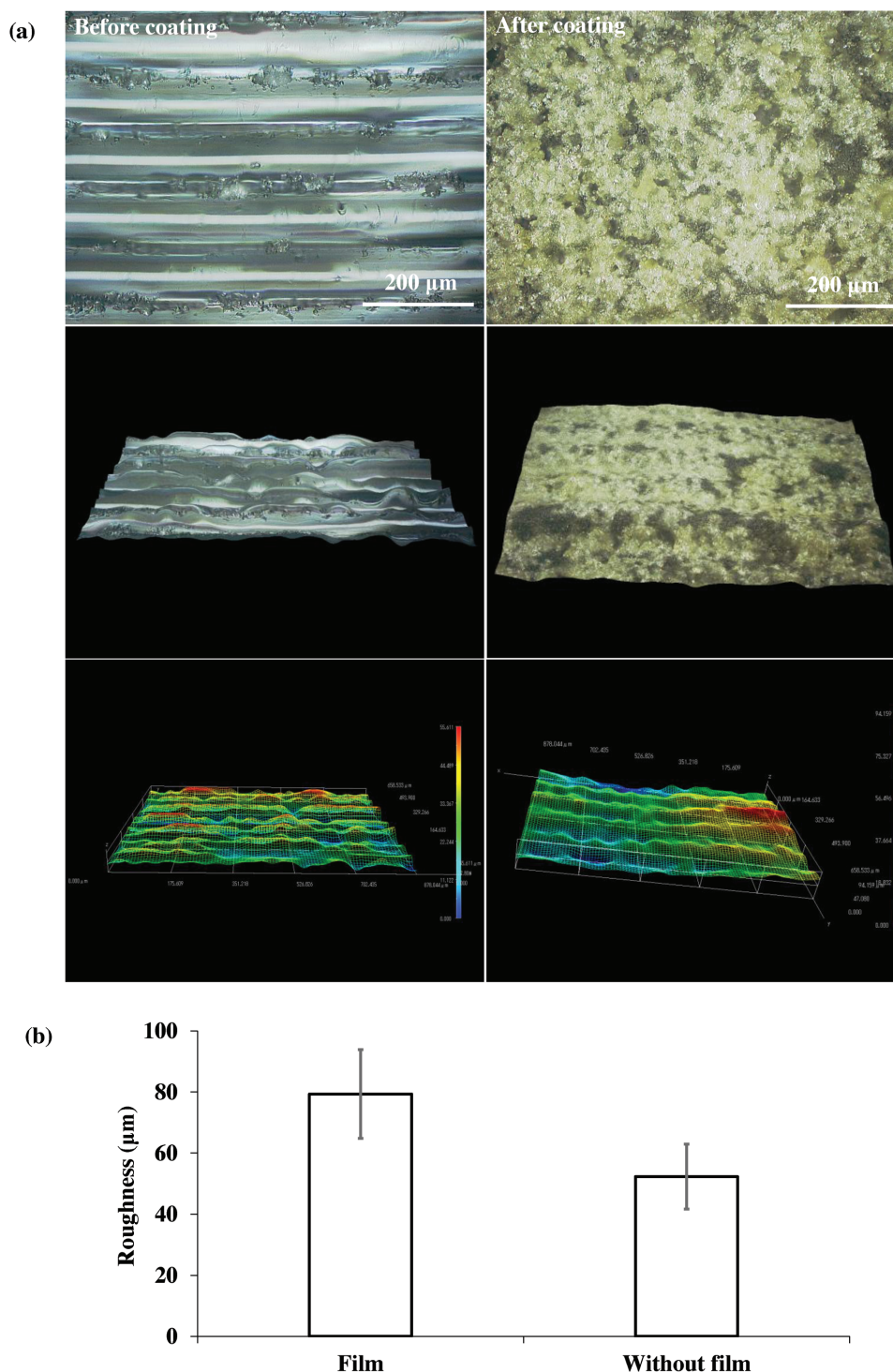
Figure 1. The a) Hirox 3D microscopy and b) 3D topographical images revealed surface properties and interior structures of DPD@zein layer. No significant difference was found in roughness of base and DPD@zein layer (b) ($n = 3$).

ΔS can be derived from the slope and intercept of Equation (3). The primary interaction can be determined as van der Waal forces and/or hydrogen bonds (if $\Delta H < 0$ and $\Delta S < 0$), electrostatic interactions (if $\Delta H < 0$ and $\Delta S > 0$), or hydrophobic forces ($\Delta H > 0$ and $\Delta S > 0$).[27] Meanwhile, $\Delta G < 0$ calculated by

Equation (4) means the interaction process is spontaneous, and $\Delta G > 0$ means the reverse reaction process is spontaneous.[27]

As shown in Table 1 and Figure 3f, both the enthalpy change ΔH and entropy change ΔS were positive. This indicated the predominance of entropy-driven interaction (i.e., hydrophobic

**ADVANCED
SCIENCE NEWS**

www.advancedsciencenews.com

**ADVANCED
MATERIALS
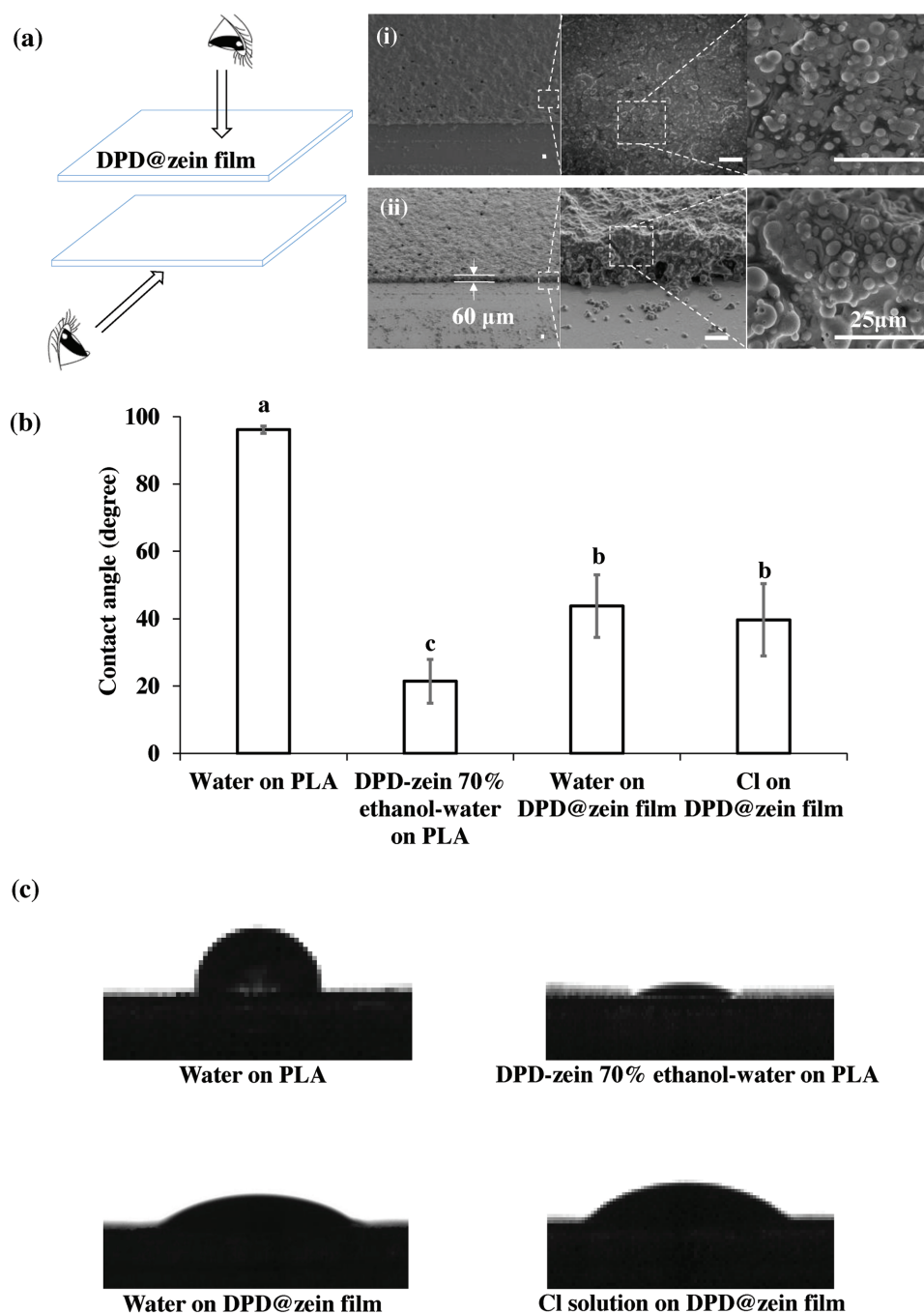INTERFACES**

www.advmatinterfaces.de

Figure 2. The FIB/SEM images (a) revealed that DPD@zein layer up surface (i) and layer interior (ii) were made up of spherical particles. The scale bars in all FIB/SEM images are 25 μm. b,c) The surface wettability of the PLA-based chip and chorine-sensing chip surfaces for water, DPD–zein 70% ethanol–water solution and 72 mg L^{-1} chlorine in 50×10^{-3} M PB aqueous solution. b) Contact angle measurement ($n = 3$), and c) Snapshot of water, DPD–zein 70% ethanol-water solution and 72 mg L^{-1} chlorine in 50×10^{-3} M PB aqueous solution droplets. The significance analysis results with different levels were noted as "a," "b," and "c" and shown in (b).

interaction) in the binding of DPD with zein.[27] The positive enthalpy change ΔH suggested the binding of DPD with zein be an endothermic process. Furthermore, the negative values for free energy ΔG at all experimental temperatures indicated that the interaction process of DPD with zein was spontaneous.[26,27]

The interaction between DPD and zein molecules on dried DPD@zein film was further investigated by FT-IR spectroscopy.

As shown in Figure S1 (Supporting Information), two major bands were observed for zein at 1641 (amide I, C=O vibration) and 1529 cm^{-1} (amide II, N—H vibration) due to the peptide bonds.[28,29] Upon incorporation of DPD, a marked blue shift to 1537 cm^{-1} was observed in the amide II band, whereas no shift of the amide I band was found. Moreover, the characteristic peak at 3286 cm^{-1} (O—H stretch)[30] exhibited a slight blue shift
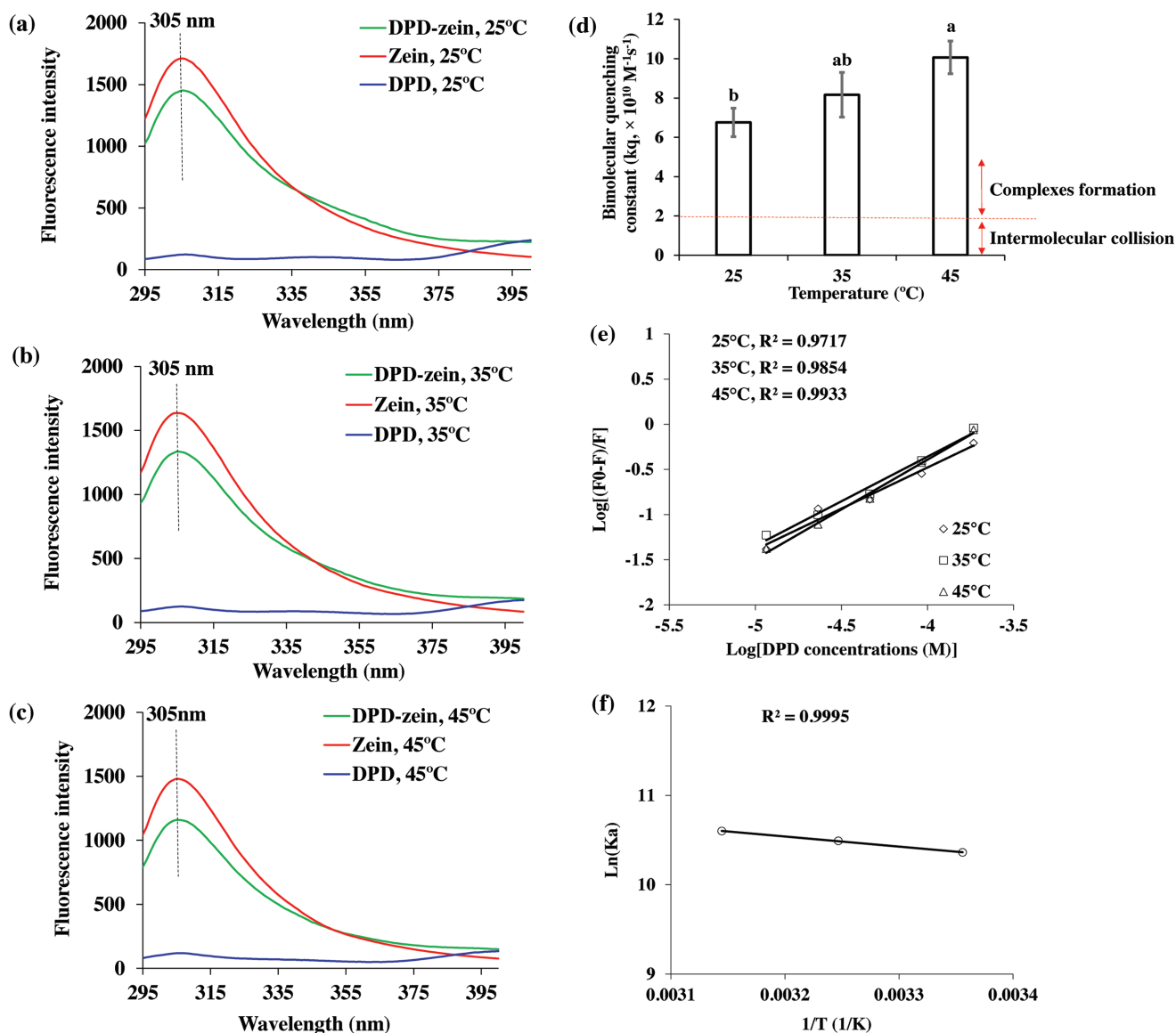
Figure 3. The change of the fluorescence intensity of zein before and after mixing with DPD in 70% ethanol–water solution at temperatures of a) 25, b) 35, and c) 45 °C. d) The fluorescence quenching constant (k_q) of zein by DPD at 25, 35, and 45 °C was also analyzed by the Stern–Volmer model to confirm the presence of dynamic or static quenching. e) The plot of $\log[(F_0 - F)/F]$ as a function of log value of DPD concentration (mol L^{-1}), and f) the Van't Hoff plot of ln K as a function of 1/T (K) were calculated to reveal the interaction of zein and DPD molecules.

to 3289 cm^{-1} after the addition of DPD. Based on the FT-IR results, the amine and hydroxyl groups on zein played important roles in binding with DPD, probably through hydrogen

Table 1. The binding constant (K_a) and number of binding sites (n) of DPD with the fluorophore of zein at temperatures of 25, 35, and 45 °C. The enthalpy (ΔH), entropy (ΔS), and free energy (ΔG) change based on the van't Hoff equation.

T [°C]	K_a [10^4 M^{-1}]	n	R^2	ΔH [J mol^{-1}]	ΔS [J mol^{-1} K^{-1}]	ΔG [J mol^{-1}]
25	3.2	0.9099	0.9717			−3088.2
35	3.6	0.9877	0.9854	1129.1	14.2	−3229.7
45	4.0	1.1008	0.9933			−3371.2

bonding. The contribution of hydrophobic interaction in the dry film was expected to be low, as the low water content in the film favors hydrogen bonding and weakened the hydrophobic interaction considerably. Collectively, these interactions resulted in a successful incorporation of DPD in the zein matrix, as revealed by the X-ray diffraction (XRD) results (Figure S2, Supporting Information).

2.3. Coloration of Chlorine-Sensing Chip

The DPD is a commonly used reagent to detect free chlorine because of the reaction of DPD with chlorine to generate a magenta-colored semiquinoid cationic compound,[15] which is
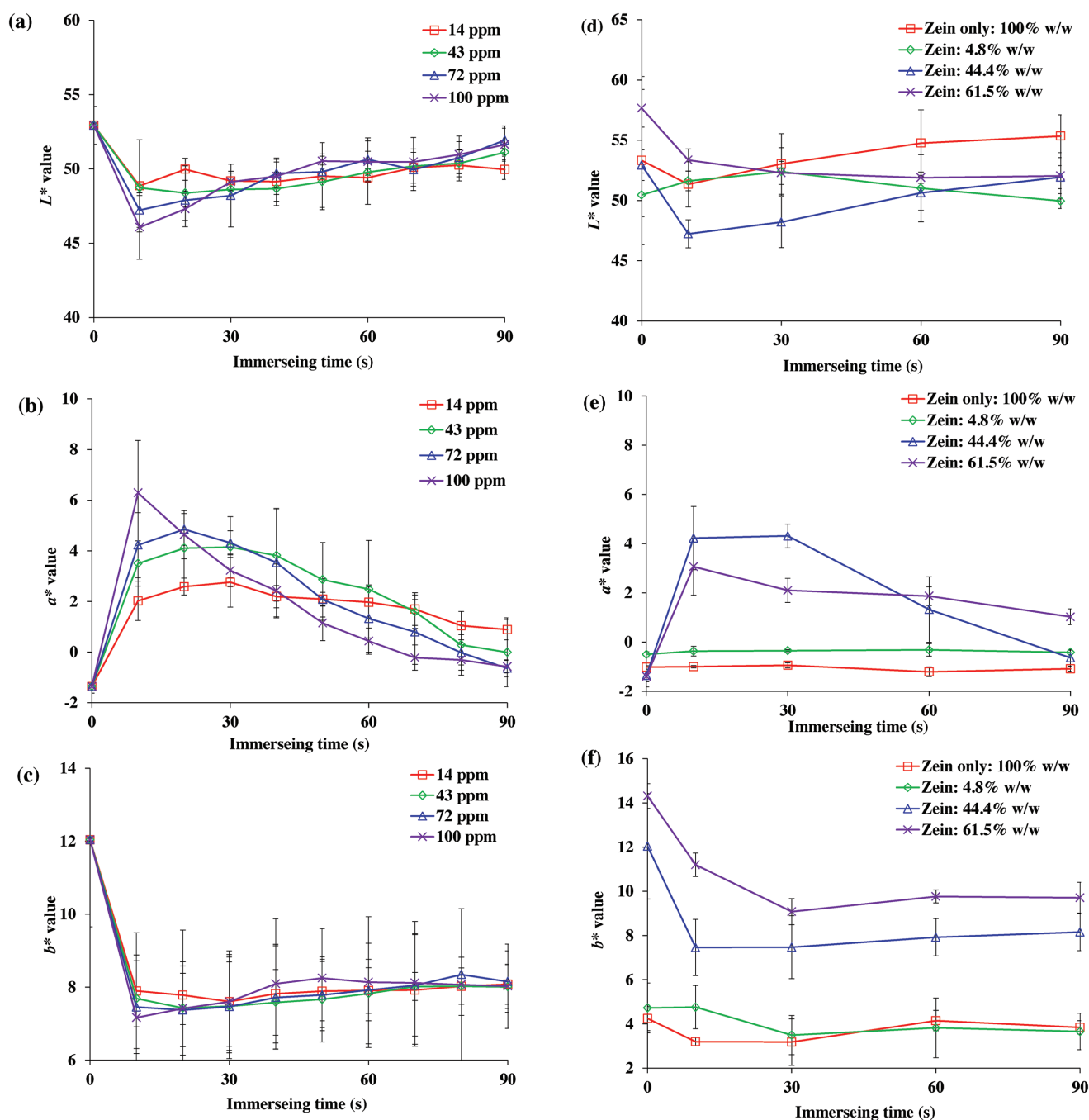
ADVANCED
SCIENCE NEWS
www.advancedsciencenews.com

ADVANCED
MATERIALS
INTERFACES
www.advmatinterfaces.de

Figure 4. The *L**, *a**, and *b** values (a, b, and c) of chlorine-sensing chip dynamic coloration in chlorine aqueous solution at chlorine concentrations of 14, 43, 72, and 100 mg L^{-1}. *L**, *a**, and *b** values (d, e, and f) of chlorine-sensing chip coated by DPD@zein film at zein mass ratios of 4.8% w/w, 44.4% w/w, 61.5% w/w, and 100% w/w (zein only, as control) (*n* = 3).

able to be distinguished in the visible spectrum. The coloration of the chlorine-sensing chip was assessed as a function of free available chlorine (FAC) level, immersion time, and zein concentration. As shown in **Figure 4**a–c, the lightness (*L** value) and yellowness (*b** value) of the chlorine-sensing chip decreased remarkably in the first 10 s, followed by a slow increase from 50 to 80 s until an equilibrium was reached at 90 s. The redness (*a** value) increased to a maximum at 10–30 s

depending on the FAC level and then decreased gradually. The initial increase and subsequent decrease in the redness may be ascribed respectively to the formation of magenta DPD–chlorine complex and its discoloration through further chlorination. In the presence of excessive free chlorine, the DPD–chlorine complex is further oxidized to a relatively unstable, colorless imine compound.[31] The significant decrease in redness at higher FAC levels was attributable to the excess chlorine that

led to rapid discoloration. As for the concentration dependence, an increase in $a*$ was observed as the FAC level increased from 14 to 72 mg L^{-1}. However, a higher level of FAC at 100 mg L^{-1} resulted in a significant reduction in the redness, which was also attributable to the discoloration reaction. Although a weak coloration occurred at chlorine concentration of 14 mg L^{-1}, a stable magenta-colored duration time was observed after the first 10 s. That indicated the detection limit of the chip for chlorine at lower than 14 mg L^{-1} in pH 6.5 PB solution. However, to pinpoint the exact detection limit, more experiments at low chlorine concentrations are needed. Since the changes of $L*$, $a*$, and $b*$ values in Figure 4a after 30 s of immersing were not statistically significant, the fluctuation was thought to be caused by the experimental error. Another reason for the fluctuation of $L*$ value might be the instability of brightness of the sensing chip. The smallest variations of redness ($a*$) and yellowness ($b*$) from 30 to 90 s were found at lowest chlorine concentration (i.e., 14 mg L^{-1}). It indicated that coloration was more stable at lower chlorine concentrations.

Figure 4d–f shows the colorimetric profile of chlorine sensing chip as a function of zein concentration at an FAC level of 72 mg L^{-1}. Overall, no significant change in $L*$ value was found among the films containing 4.8, 44.4, and 61.5% zein, but significant differences were observed in $a*$ and $b*$ values. Higher redness was observed at 44.4% zein than at 61.5% zein, whereas no color was observed with 4.8% zein. The abundant chlorine-reactive residues such as tyrosine, lysine and arginine in zein may compete for chlorine with DPD.[16]

Based on this information, we speculated that at low concentrations, zein did not significantly deplete FAC and thus exposed DPD to a high concentration of FAC and facilitated discoloration. On the other hand, at high concentration, zein competed with DPD for reacting with FAC, leading to a slower formation rate of the colored DPD–chlorine complex. In summary, the data indicated that the zein solid content of 44.4% w/w was suitable for chlorine-sensing chip coloration in 72 mg L^{-1} chlorine aqueous solution, and was therefore applied in the chlorine permeation investigation.

2.4. Chlorine Permeation in Lab- and Pilot-Industrial Scale Systems

As shown in **Figure 5**a and Figures S3 and S4 (Supporting Information), for full-depth cracks that penetrated the chip, chlorine permeated more effectively when the crack was oriented perpendicular to liquid level than when it was parallel. This result was likely due to insignificant blocking of chlorine permeation by aerial cavities (bubbles) formed in the cracks that were perpendicular to the liquid level. A relatively stable aerial cavity was probably generated when the chlorine-sensing chip was immersed with the crack parallel to the liquid level. In this instance, both sides of the chip crack would be at the same liquid level resulting in equal hydraulic pressure.[32] In contrast, immersing the chlorine-sensing chip into an aqueous solution with the crack perpendicular to the liquid level facilitated the
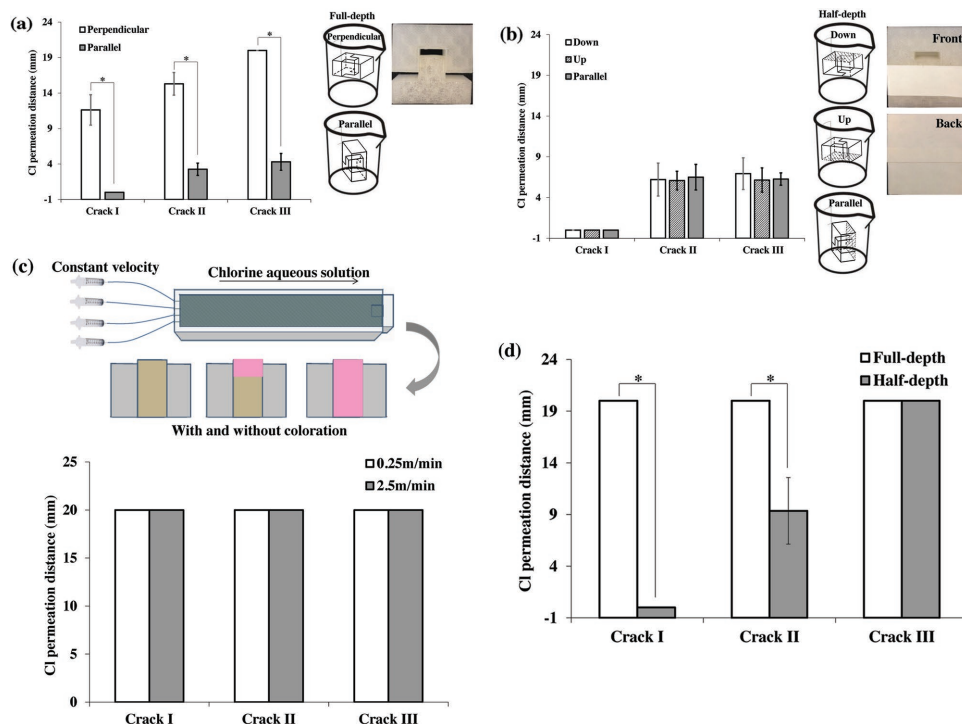

Figure 5. The chlorine permeation distance into cracks I, II, and III with crack width of 0.2, 0.5, and 1.0 mm, respectively. The chlorine permeation was tested at static chlorine aqueous solution with a) full-depth and b) half-depth cracks, c) at dynamic chlorine aqueous solution with vertical flow velocity of 0.25 and 2.5 m min^{-1} (Re of 12.5 and 125), and in a d) Meyer pilot-industrial scale vegetable washer at chlorine concentration of 72 mg L^{-1} (*$p < 0.05$, $n = 5$). In order to clearly show the structure of full-depth and half-depth cracks, images of 3D-printed chips with crack width of ≈30 mm (used for clearly presentation) were presented along with the sketches.

discharge of air from the cavity because of the difference in hydraulic pressure on the two sides of the chip crack.

The chlorine permeation into half-depth cracks was further studied and shown in Figure 5b and Figures S5 and S6 (Supporting Information). No permeation was observed in the crack with 0.2 mm width, which was probably because liquid could only penetrate from one side. Increasing crack width to 0.5 and 1.0 mm facilitated chlorine permeation, allowing it to diffuse by 6.1 and 6.9 mm respectively without significant difference.

The dynamic chlorine permeation of the chlorine solution flow velocity of 0.25 and 2.5 m min^{-1} was investigated to further study the water flow pattern occurring during fresh produce washing and to reveal the gravity effects and/or the Bernoulli layer surface effects. The fluid state of chlorine solution can be calculated based on the Reynolds number (Equation (5)).[33]

$$Re = \frac{\rho v l}{\mu} \tag{5}$$

where, Re is the Reynolds number, ρ is the density of the fluid (kg m^{-3}), approximately equal to 1.0×10^3 kg m^{-3}, v is the velocity of the fluid with respect to the object (m s^{-1}), μ is the dynamic viscosity of the fluid (kg (m s)$^{-1}$), approximately equaling to the viscosity of water at 20 °C of 1.0×10^{-3} kg (m s)$^{-1}$, and l is separation distance between plates (m), i.e., the plate distance of groove, 3.0×10^{-3} m, in the present study.

The Re corresponding to this study was 12.5 or 125 at velocities of 0.25 or 2.5 m min^{-1}, respectively. A Re below 2.1×10^3 suggests a complete laminar flow state of chlorine solution passing through the border of cracks.[34] The dynamic chlorine permeation protocol is designed to mimic the hydrodynamics characteristics when fluid flows through the upper side of chlorine-sensing chip cracks, like models undergoing transverse vortex-induced vibration[35] in pilot-industrial scale vegetable washer. As shown in Figure 5c and Figures S7 and S8 (Supporting Information), coloration was observed throughout the chip crack with the width of 0.2 mm, while no color remnant (because of overchlorination, Figure S8, Supporting Information) was shown at a crack width of 0.5 and 1.0 mm. The permeation of chlorine solution from the upper side of cracks into the interior was driven by gravity, finally producing complete permeation within 30 s of dynamic washing process. Moreover, boundary pressure produced by chlorine solution flowing through the side of the cracks at Re of 12.5 and 125 (the velocity of 0.25 and 2.5 m min^{-1}) was calculated by the Bernoulli equation (Equations (6) and (7))[36]

$$B_c = \frac{v^2}{2} + gh + \frac{p}{\rho} \tag{6}$$

$$p = -\frac{\rho v^2}{2} - \rho gh - \rho B_c \tag{7}$$

where v is the velocity of the fluid (m s^{-1}), g is the gravity acceleration (m s^{-2}), h is the elevation of the point above a reference plane (i.e., the height of fluid above the crack side) (m), p is the boundary pressure at the experimental point (kg (m s^2)$^{-1}$), ρ is the density of the fluid (kg m^{-3}), and B_c is the Bernoulli constant.[36]

According to Equation (7), chlorine permeation generated by chlorine solution flowing through the upper side of the cracks should have been facilitated at the lower flow velocity of 0.25 m min^{-1} (Re of 12.5) relative to that at the higher velocity of 2.5 m min^{-1} (Re of 125), although no difference of chlorine distance was found from the results in Figure 5c. That was probably caused by the complete laminar flow state of both of the chlorine solution at lower Re of 12.5 and 125 comparing to the complete laminar critical value of 2.1×10^3.[34]

Furthermore, a pilot-industrial scale produce washer was used to investigate the chlorine permeation during 30 s wash to mimic industrial washing process. As shown in Figure 5d and Figures S9 and S10 (Supporting Information), chlorine permeated through the full-depth cracks with all widths (i.e., 0.2, 0.5, and 1.0 mm). However, no chlorine permeated into half-depth crack at a crack width of 0.2 mm. Increasing half-depth crack width to 0.5 and 1.0 mm facilitated chlorine permeation, leading to permeation distances of 9.4 and full crack depth of 20 mm, respectively. Thus, the pilot indus-trial produce washer resulted in significantly more effective chlorine permeation than was observed for the static chlorine solution.

3. Conclusions

A novel 3D printed base chip was developed and fabricated with separable artificial cracks. Coating a DPD–zein layer with surface roughness of 79.3 µm and average thickness of 60 µm onto the base chip generated a chlorine-sensing functionality. The layer surface showed an affinity of chlorine aqueous solution with contact angle of 39.7°. The primary interaction of zein and DPD in layer was hydrogen binding evidenced by the blue shift of the amide II band of zein. This chlorine-sensing chip showed a stable magenta color within 30 s immersion in 72 mg L^{-1} chlorine aqueous solution, which was employed to probe the chlorine permeation in both lab-scale static or dynamic conditions and a pilot-industrial scale commercial vegetable wash system. Under lab-scale conditions, chlorine permeation into full-depth chip at crack width of 0.2, 0.5, and 1.0 mm was 11.6, 15.3, and 20.0 mm respectively, when the cracks were perpendicular to liquid level. Meanwhile, the permeation distances were decreased to 0, 3.3, and 4.3 mm from both two sides of crack when the cracks were parallel to liquid level. Immersing chip into chlorine solution showed insignificant difference of permeation distance with half-depth cracks of down, up, and parallel to liquid level. In this case, the chlorine permeation distance was 0 mm at the crack width of 0.2 mm, and increased to 6.1 and 6.9 mm when the crack width changed to 0.5 and 1.0 mm, respectively. Additionally, complete chlorine permeation (20 mm) was detected after dynamic washing of chlorine-sensing chip in a groove for 30 s at the Re numbers of chlorine solution of 12.5 and 125. In a pilot-industrial scale condition, complete chlorine permeation (20 mm) was detected in full-depth chlorine-sensing chip, while, permeation distance was 0, 9.4, and 20 mm in half-depth chip at crack width of 0.2, 0.5, and 1.0 mm. In brief, the chlorine-sensing chip is a useful platform to study the sanitizer efficacy in hard-to-reach locations during the washing process.

4. Experimental Section

Materials and Chemicals: DPD reagent was purchased from HF Scientific (Fort Myers, FL, USA), zein (nitrogen content 13.85% w/w) from MP Biomedicals (Solon, OH, USA), and ethyl alcohol 200 proof from Pharmco-Aaper (Shelbyville, KY, USA). Bleach solution containing 7.85% sodium hypochlorite was obtained from Clorox (Oakland, CA, USA).

3D Printing Base and Fabricating Chlorine-Sensing Chips: A 3D replicator/printer (MakerBot 3D Printing Company, NY, USA) was used to design and print the PLA-based chip consisting of two interlocking and detachable components, as illustrated in **Figure 6**a,b. A gap with 0.2–10 mm width is present between the two parts when locked, mimicking the cracks and crevices found in nature on fresh produce.[37] The cracks by design extended through either the entire depth or one-half of the depth of the chip to simulate cracks and crevices of varying depths.

The chlorine-sensing layer was prepared by a solution of 80 mg of zein dissolved in 10 mL 70% ethanol–water (v/v) solution with 100 mg DPD added under constant nitrogen flow. After sonicating for 10 min in a Branson 5510 ultrasonicator (Branson Ultrasonics Co., Danbury, CT, USA), an aliquot of 200 µL of the resulting dispersion was dripped on the "male" part of the chip (total surface area 200 mm^2, Figure 6c) and air-dried at 21 °C. Thus formed zein film was defined as DPD@zein film.

Morphology and Surface Topography of Chlorine-Sensing Film and Based PLA Chip: The surface topography of the DPD@zein film and the PLA base was examined with a Hirox KH-77003D digital optical microscope (Hirox Co. Ltd., Hackensack, NJ, USA). The 3D data were further processed to generate dimensional-structural models and to calculate surface roughness. The surface and cross-section of the DPD@zein layer prepared by dripping 69.2 µL DPD–zein dispersion on a 69.2 mm^2 silicon slice surface (equivalently 200 µL DPD–zein dispersion on 200 mm^2 base chip) and drying in air were further observed using a FEI 620 dual-beam focus ion beam scanning electron microscopes (FIB/SEM, FEI, Eindhoven, The Netherlands) at the voltage of 10 kV without coating gold.

Measurement of Surface Hydrophobicity: Contact angle measurement of DPD–zein mixture-coated surface was performed by the sessile drop method using an Attension Theta optical tensiometer (Biolin Scientific, Linthicum Heights, MD, USA), with a drop volume of 50 µL (5 drops on a 1 cm × 10 cm strip). Placement of drops was controlled by a C201 automatic liquid dispenser (Biolin Scientific). An aliquot of 20 µL either 70% aqueous ethanol, 72 mg L^{-1} free chlorine solution or pure di-water was dropped onto PLA or DPD@zein film. Data collection (60 fps) was manually triggered by the initial contact of a liquid drop with a solid surface. Captured images were automatically analyzed by an OneAttension software, Version 1.8 (Biolin Scientific) to identify the baseline and calculate contact angles.

Determination of the Intermolecular Interaction Mechanism: The interactions involved in the interactions between DPD and zein in 70% ethanol aqueous solution were studied using the fluorescence spectrum using a RF-1501spectrofluorometer (Shimadzu Corp., Tokyo, Japan). Samples were measured at 25, 35, or 45 °C, using a fixed excitation wavelength of 280 nm and varied emission wavelengths ranging from 295 to 400 nm.

The chemical interaction between zein and DPD in dry DPD@zein film was investigated via a Fourier transform infrared spectroscopy (FT-IR) analysis using a Jasco FT/IR-4100 (JASCO Co., Ltd, Tokyo, Japan). The spectrum was obtained by 32 repeated scans from 4000 to 600 cm^{-1} at a resolution of 2 cm^{-1}, with background deducted by the software.

Dynamic Coloration of Chlorine-Sensing Chip: The chlorine-sensing chips were immersed in phosphate buffer (PB, 50 mmol L^{-1}, pH 6.5) solutions with FAC levels of 14, 43, 72, and 100 mg L^{-1} measured using a CP-15 free chlorine photometer (HF Scientific Inc., Ft. Myers, FL). After immersion, the chips were measured immediately every 10 s for their colorimetric profiles (*L**, *a**, and *b** values) using a CR-400 Chroma Meter (Konica Minolta Sensing, Inc., Osaka, Japan).
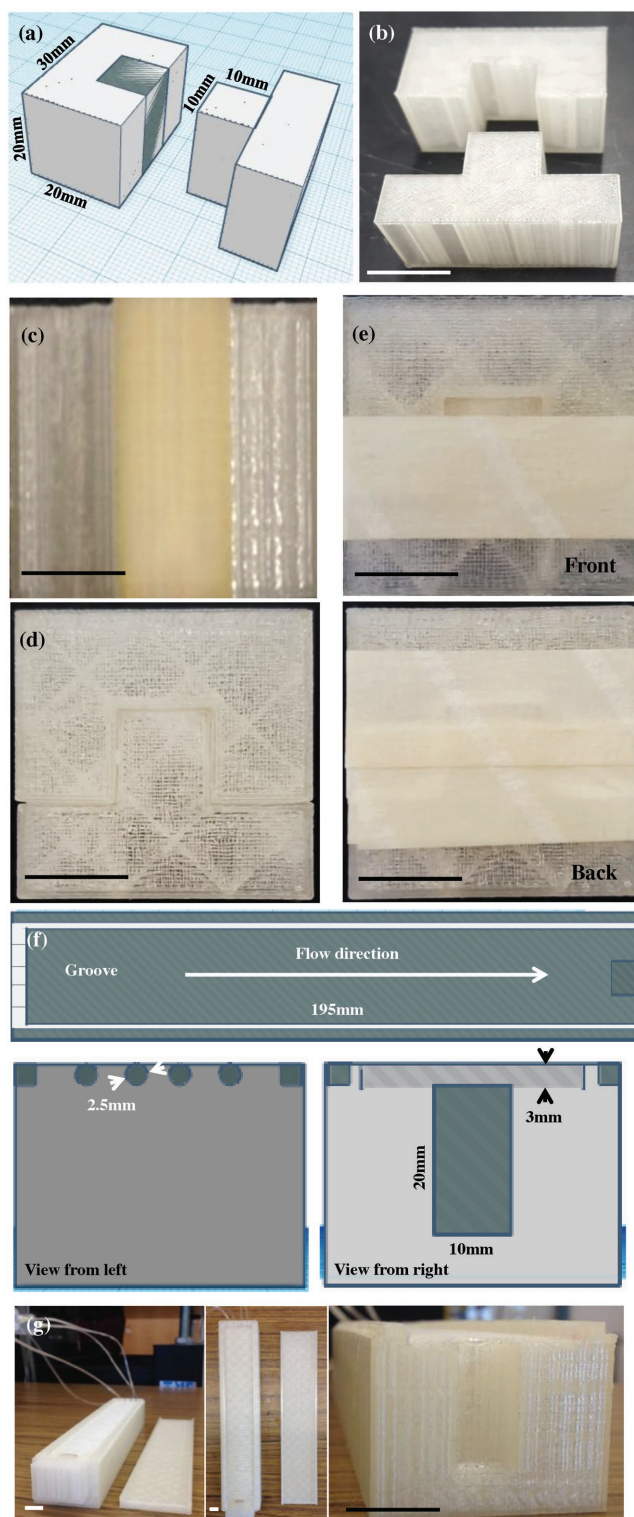

Figure 6. The a) design and b) model of PLA-based chip using 3D printing. c) A layer of DPD@zein film was coated on the "male" surface of the base chip. The d) full-depth and e) half-depth chlorine-sensing chips were used to understand the chlorine permeation. The f) design and g) model of PLA-based groove for producing fluid with constant flow rate vertically flowing through the border of penetrating cracks. The scale bar is 10 mm showing in the optical images.
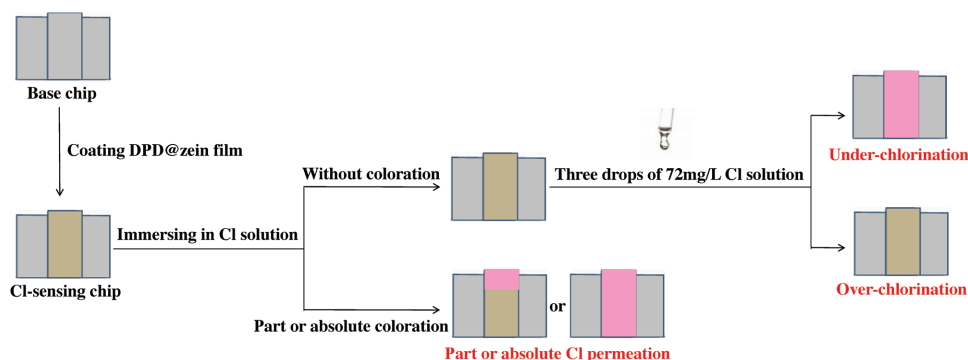
Figure 7. The schematic diagram of the application of chlorine sensing chip to determine the chlorine permeation.

The chlorine-sensing chips with zein contents of 4.8, 44.4, and 61.5% (corresponding to zein concentrations of 0.5, 8, and 16 mg mL^{-1} in the coating solution) were immersed in PB solutions (50 mmol L^{-1}, pH 6.5) containing 72 mg L^{-1} FAC. After immersion, the chips were measured immediately every 30 s. The zein film fabricated from 8 mg mL^{-1} zein solution without DPD was coated on a 3D base chip as a control.

Chlorine Permeation Measurement: Lab-scale static chlorine permeation was studied by using the chlorine-sensing chip with optimal film formula containing 44.4% zein and 55.6% DPD (w/w) (Figure 6d,e) located 30 mm below the liquid level of 72 mg L^{-1} chlorine solution. In addition, to investigate the lab-scale dynamic chlorine permeation under a flowing solution, a PLA-matrical groove was developed (Figure 6f,g) to allow 72 mg L^{-1} chlorine solution flowing along the length of the groove at a velocity of 0.25 or 2.5 m min^{-1} for 30 s using a Fusion 720 syringe pump (Chemyx Inc., Stafford, TX, USA). The dynamic chlorine solution vertically flowed through the upper side of chlorine-sensing chip cracks coating same film with 44.4% zein and 55.6% DPD (w/w) to understand the effects of boundary pressure on chlorine permeation. After immersion in static or dynamic chlorine solutions, the chips were measured for the chlorine-diffused distance by the indicated magenta band from the upper side of crack to the end of magenta band based on the procedure in the *Chlorine Permeation into Chlorine-sensing Chip* section below.

The chlorine-sensing chip was further tested in an industrial-scaled vegetable wash system (Meyer Industries, Inc., San Antonio, TX, USA). The vegetable washer has a capacity of 3000 L and uses an air agitation. The wash water was chlorinated at a free chlorine concentration of 72 mg L^{-1}. During washing, chlorine solution was pumped from a flume, and slowly flowed in the vegetable washer unidirectionally, which was then introduced back into the flume. The chlorine-sensing chip was placed into the wash water where they were washed for 30 s, a common wash practice for fresh-cut vegetables. The cracks were examined for chlorine permeation as described for the procedure in the *Chlorine Permeation into Chlorine-sensing Chip* section below.

Chlorine Permeation into Chlorine-Sensing Chip: The procedure for the chlorine permeation test is shown in **Figure 7**. Briefly, the chlorine-sensing chip was immersed in aqueous chlorine solution for 30 s, and then separated into two parts at the gap (simulating cracks or crevices) to measure the depth of the chlorine permeation via the magenta band. If no coloration was observed on the surface of the cracks, three drops of chlorine aqueous solution were added on the film to discern whether the colorlessness was caused by over-chlorination or under-chlorination.

Statistical Analysis: The contact angle and fluorescence spectrum measurements were carried out in triplicate. Chlorine permeation measurement was conducted with five replicates. Data were reported as mean ± standard deviation (SD). The independent-samples *t* test was used to determine any significant differences ($p < 0.05$) of

surface roughness between base and chlorine-sensing chips. Analysis of variance (ANOVA) with the Duncan method followed by multiple post hoc comparisons were carried out to determine any significant differences ($p < 0.05$) using the Statistical Product and Service Solutions (SPSS) 16.0 software (SPSS Inc., Chicago, IL, USA).

Supporting Information

Supporting Information is available from the Wiley Online Library or from the author.

Conflict of Interest

The authors declare no conflict of interest.

[1] a) S. Van Boxstael, I. Habib, L. Jacxsens, M. De Vocht, L. Baert, E. Van de Perre, A. Rajkovic, F. Lopez-Galvez, I. Sampers, P. Spanoghe, B. De Meulenaer, M. Uyttendaele, *Food Control* **2013**, *32*, 190; b) M. Lynch, R. Tauxe, C. Hedberg, *Epidemiol. Infect.* **2009**, *137*, 307.

[2] J. Barbosa, M. Cuppini, J. Flach, C. Steffens, R. Cansian, G. Toniazzo, *LWT-Food Sci. Technol.* **2016**, *71*, 309.

[3] a) A. Shallan, P. Smejkal, M. Corban, R. Guijt, M. Breadmore, *Anal. Chem.* **2014**, *86*, 3124; b) Y. Mishnayot, M. Layani, I. Cooperstein, S. Magdassi, G. Ron, *Rev. Sci. Instrum.* **2014**, *85*, 085102.

[4] a) G. Gu, I. Su, S. Sharma, J. Voros, Z. Qin, M. Buehler, *J. Biomech. Eng.* **2016**, *138*, 021006; b) B. Hung, B. Naved, E. Nyberg, M. Dias, C. Holmes, J. Elisseeff, A. Dorafshar, W. Grayson, *ACS Biomater. Sci. Eng.* **2016**, *2*, 1806.

[5] a) S. Murphy, A. Atala, *Nat. Biotechnol.* **2014**, *32*, 773; b) B. Gross, J. Erkal, S. Lockwood, C. Chen, D. Spence, *Anal. Chem.* **2014**, *86*, 3240; c) W. Zhu, X. Ma, M. Gou, D. Mei, K. Zhang, S. Chen, *Curr. Opin. Biotechnol.* **2016**, *40*, 103.

[6] a) R. Walczak, K. Adamski, *J. Micromech. Microeng.* **2015**, *25*, 085013; b) J. Lind, T. Busbee, A. Valentine, F. Pasquali, H. Yuan, M. Yadid, S. Park, A. Kotikian, A. Nesmith, P. Campbell, J. Vlassak, J. Lewis, K. Parker, *Nat. Mater.* **2017**, *16*, 303.

[7] G. Salentijn, P. Oomen, M. Grajewski, E. Verpoorte, *Anal. Chem.* **2017**, *89*, 7053.

[8] H. Ota, S. Emaminejad, Y. Gao, A. Zhao, E. Wu, S. Challa, K. Chen, H. Fahad, A. Jha, D. Kiriya, W. Gao, H. Shiraki, K. Morioka, A. Ferguson, K. Healy, R. Davis, A. Javey, *Adv. Mater. Technol.* **2016**, *1*, 1600013.

[9] A. Ambrosi, M. Pumera, *Chem. Soc. Rev.* **2016**, *45*, 2740.

[10] J. Lunt, *Polym. Degrad. Stab.* **1998**, *59*, 145.

[11] H. Chia, B. Wu, *J. Biol. Eng.* **2015**, *9*, 4.

[12] J. Russias, E. Saiz, S. Deville, K. Gryn, G. Liu, R. Nalla, A. Tomsia, *J. Biomed. Mater. Res. A* **2007**, *83A*, 434.

[13] D. Stout, B. Basu, T. Webster, *Acta Biomater.* **2011**, *7*, 3101.

[14] a) D. Gombas, Y. Luo, J. Brennan, G. Shergill, R. Petran, R. Walsh, H. Hau, K. Khurana, B. Zomorodi, J. Rosen, R. Varley, K. Deng, *J. Food Prot.* **2017**, *80*, 312; b) Y. Luo, S. Hauteb, X. Nou, B. Zhang, Z. Teng, E. Turner, Q. Wang, P. Millnera, *Food Microbiol.* **2018**, *70*, 120.

[15] L. Moberg, B. Karlberg, *Anal. Chim. Acta.* **2000**, *407*, 127.

[16] E. Gianazza, V. Viglienghi, P. Righetti, F. Salamini, C. Soave, *Phytochemistry* **1977**, *16*, 315.

[17] L. Wang, T. Gotoh, Y. Wang, T. Kouyama, J. Wane, *J. Phys. Chem. C* **2017**, *121*, 19999.

[18] J. Liang, H. Yan, X. Wang, Y. Zhou, X. Gao, P. Puligundla, X. Wan, *Food Chem.* **2017**, *231*, 19.

[19] J. Li, R. Zhang, *Sci. Rep.* **2016**, *6*, 22304.

[20] B. Zhang, A. Feldman, Q. Wang, *Sens. Actuators, B* **2013**, *186*, 597.

[21] K. Pan, Q. Zhong, S. Baek, *J. Agric. Food Chem.* **2013**, *61*, 6036.

[22] Y. Zhang, Q. Zhong, *J. Agric. Food Chem.* **2012**, *60*, 1880.

[23] I. Joye, G. Davidov-Pardo, R. Ludescher, D. McClements, *Food Chem.* **2015**, *185*, 261.

[24] S. Lehrer, *Biochemistry* **1971**, *10*, 3254.

[25] D. Acharya, L. Sanguansri, M. Augustin, *Food Chem.* **2013**, *141*, 1050.

[26] Y. Hu, Y. Liu, H. Wang, X. Xiao, S. Qu, *J. Pharm. Biomed. Anal.* **2004**, *36*, 915.

[27] P. Ross, S. Subramanian, *Biochemistry* **1981**, *20*, 3096.

[28] a) A. Alcantara, P. Aranda, M. Darder, E. Ruiz-Hitzky, *J. Mater. Chem.* **2010**, *20*, 9495; b) A. Unnithan, G. Gnanasekaran, Y. Sathishkumar, Y. Lee, C. Kim, *Carbohydr. Polym.* **2014**, *102*, 884.

[29] H. Guo, T. Kimura, Y. Furutani, *Chem. Phys.* **2013**, *419*, 8.

[30] F. Garczarek, K. Gerwert, *Nature* **2006**, *439*, 109.

[31] H. Moore, M. Garmendia, W. Cooper, *Environ. Sci. Technol.* **1984**, *18*, 348.

[32] M. Perera, P. Ranjith, S. Choi, D. Airey, *Fuel* **2011**, *90*, 547.

[33] K. Seshadri, F. Williams, *Int. J. Heat Mass Transfer* **1978**, *21*, 251.

[34] A. Pavelyev, A. Reshmin, S. Teplovodskii, S. Fedoseev, *Fluid Dyn.* **2003**, *38*, 545.

[35] R. Tumkur, A. Pearlstein, A. Masud, O. Gendelman, A. Blanchard, L. Bergman, A. Vakakis, *J. Fluid Mech.* **2017**, *828*, 196.

[36] M. Saleta, D. Tobia, S. Gil, *Am. J. Phys.* **2005**, *73*, 598.

[37] a) B. Zhang, Y. Luo, A. Pearlstein, J. Aplin, Y. Liu, G. Bauchan, G. Payne, Q. Wang, X. Nou, P. Millner, *ACS Appl. Mater. Interfaces* **2014**, *6*, 12467; b) D. Gautam, S. Dobhal, M. Payton, J. Fletcher, L. Ma, *PloS One* **2014**, *9*, e105248.